Research in Nondestructive Evaluation
Publication details, including instructions for authors and subscription information:
http://www.tandfonline.com/loi/urnd20

Cork Embedded Internal Features and Contrast Mechanisms with Dei Using 18, 20, 30, 36, and 40 keV Synchrotron X-Rays

V. Rao Donepudi [a], Roberto Cesareo [a], Antonio Brunetti [a], Zhong Zhong [b], Tetsuya Yuasa [c], Takao Akatsuka [c], Tohoru Takeda [d] & Giovanni E. Gigante [e]

[a] Istituto di Matematica e Fisica, Universita di Sassari, Sassari, Italy

[b] National Synchrotron Light Source, Brookhaven National Laboratory, Upton, New York, USA

[c] Department of Bio-System Engineering, Faculty of Engineering, Yamagata University, Yonezawa, Japan

[d] Institute of Clinical Medicine, University of Tsukuba, Tsukuba, Japan

[e] Dipartimento di Fisica, Universita di Roma "La Sapienza", Rome, Italy

Available online: 02 Aug 2010

To cite this article: V. Rao Donepudi, Roberto Cesareo, Antonio Brunetti, Zhong Zhong, Tetsuya Yuasa, Takao Akatsuka, Tohoru Takeda & Giovanni E. Gigante (2010): Cork Embedded Internal Features and Contrast Mechanisms with Dei Using 18, 20, 30, 36, and 40 keV Synchrotron X-Rays, Research in Nondestructive Evaluation, 21:3, 171-183

To link to this article: http://dx.doi.org/10.1080/09349847.2010.493990

Research in Nondestructive Evaluation, 21: 171–183, 2010

ISSN: 0934-9847 print/1432-2110 online
DOI: 10.1080/09349847.2010.493990

Taylor & Francis
Taylor & Francis Group

CORK EMBEDDED INTERNAL FEATURES AND CONTRAST MECHANISMS WITH DEI USING 18, 20, 30, 36, AND 40 KEV SYNCHROTRON X-RAYS

V. Rao Donepudi,[1] Roberto Cesareo,[1] Antonio Brunetti,[1] Zhong Zhong,[2] Tetsuya Yuasa,[3] Takao Akatsuka,[3] Tohoru Takeda,[4] and Giovanni E. Gigante[5]

[1]Istituto di Matematica e Fisica, Universita di Sassari, Sassari, Italy
[2]National Synchrotron Light Source, Brookhaven National Laboratory, Upton, New York, USA
[3]Department of Bio-System Engineering, Faculty of Engineering, Yamagata University, Yonezawa, Japan
[4]Institute of Clinical Medicine, University of Tsukuba, Tsukuba, Japan
[5]Departimento di Fisica, Universita di Roma ''La Sapienza'', Rome, Italy

Images of the cork used for wine and other bottles are visualized with the use of diffraction-enhanced imaging (DEI) technique. Present experimental studies allowed us to identify the cracks, holes, porosity, and importance of soft-matter (soft-material) and associated biology by visualization of the embedded internal complex features of the biological material such as cork and its microstructure. Highlighted the contrast mechanisms above and below the K-absorption edge of iodine and studied the attenuation through a combination of weakly and strongly attenuating materials.

Keywords: biological material, biology, cork, soft-matter, synchrotron X-rays, visualization, wine

INTRODUCTION

The behavior of X-rays as they traverse through a sample can be described using a complex index of refraction, just as in conventional optics. In the X-ray region, the index of refraction, n, deviates only slightly from unity; it can be written as $n = 1 - \delta - i\beta$, where 'β' describes the absorption of X-rays and the phase-shift term 'δ' incorporates refractive effects.

Diffraction-enhanced imaging (DEI) technique derives contrast from absorption, refraction, and extinction. Real and imaginary parts of the refractive indices are responsible for the phase-shifts and absorption for enhanced contrast imaging. For biological samples, the real part is up to 1000 times greater than the imaginary part. In this context, phase-sensitive imaging techniques are more efficient than conventional methods. It provides better

Address correspondence to V. Rao Donepudi, Department of Physics, Sir CRR Autonomous College, Elura-534007, W.G.Dt., A.P., India. E-mail: donepudi_venkateswararao@rediffmail.com

contrast, and the X-ray dose is correspondingly reduced. Recently, refraction properties of X-rays turn out to have more attractive advantages for imaging over the absorption properties. Refraction is one or two orders of magnitude more sensitive, particularly for biological and low Z materials. DEI technique exploits these refraction properties for differentiating the biological soft-tissue with high collimated synchrotron X-rays and retrieve internal structural information [1,2].

DEI technique uses a single-energy fan beam of X-rays instead of the broad energy beam used in conventional imaging. The object is scanned through the beam. The key to the new imaging method is an analyzer crystal placed between the tissue under study and the X-ray detector. The analyzer can differentiate between X-rays that are traveling much less than one ten-thousandth of a degree part. This method of line scan imaging reduces scatter and helps to visualize low-contrast areas that otherwise would be lost.

With the introduction of DEI which is capable of rendering images with absorption, refraction, and scatter rejection qualities has allowed detection of specific soft tissue based on small differences in tissue densities [3]. This new X-ray imaging technology carried out at NSLS, BNL, USA, has previously shown to allow visualization of breast tissue and a number of related medical samples explored new information [4–10].

Our experience is based at the moment on experiments that utilize high intensity synchrotron X-rays for better contrast and visualization, and rapid development of new approaches that can detect X-ray phase shifts within soft material. Some examples include, images of rat bone and lumber vertebra [11], rat spine [12] imaging applications [13], cartilage damage [14], ophthalmic diseases [15], controlled defects within bone, including bone-metal gaps [16], mass density images [17], multiple-image radiography [18–21], compositional images [22], images of seeds [23], and biological soft-tissue images [24]. For the last few years, DEI is continuously and consistently upgraded with the inclusion of new optics, electronics, mechanics and mountings, and soft-ware at various stages before imaging, at NSLS, BNL, USA. Improvements in image quality were carried out regularly on phantoms and biological samples. These studies suggest that DEI is a potential, valuable, and reliable tool for studying the refraction and scattering properties. In view of this, we applied this novel technique for the soft-materail such as cork in order to produce pure absorption and refraction images rather than two, for better understanding of the associated internal features through visualization.

The usefulness of this method was to investigate the improvement in image contrast from specimens of biological nature with synchrotron-based system. The present work is an attempt to examine an applicability of the DEI method in an exceptional case, such as, an investigation of a very light material which is difficult for examination using conventional approaches.

Indeed cork represents a demanding case since its density is very low and less absorption of X-rays.

MOTIVATION

Cork, a unique biological material, is a highly valued non-timber forest product. It is used in a variety of products, from construction materials to gaskets, but its most important use is as a stopper for premium wines. In terms of revenue, natural cork comprises one of the world's most important non-timber forest products. The principle requirements for cork stoppers are the homogeneity of the cork and the lack of cavities and/or cracks. The quality control is performed in several steps. However, most of these controls are visual checks performed by experienced people and/or by electronic cameras. All these kinds of inspection allow analyzing only the external surface. Thus little is known about the internal microstructure and cracks or holes inside the stopper will not be detected with other methods.

DEI technique is a newly developed technique for the observation of internal structures of low absorbing materials, for example in the field of structural research and application of new materials. However, the nature of interaction, namely, X-ray absorption, limited the observations only to materials having sufficient elements content. The adoption of different X-ray interaction with matter, which involves refractive properties of materials, is at the basis of DEI. DEI has demonstrated enhanced contrast for dense, highly absorbing materials of interest from medicine to material science.

This novel method allows the use of high X-ray energies, for a deeper penetration and lower dose, without losing any information on the nature of the sample. The potential use of this technique for imaging the cork and characterization may explore new information and advanced revealing features. Recent advances in tomographic data collection using synchrotron X-rays and utilization of DEI will be a new tool.

The basic physical interaction is the refraction, taking place at any boundaries between different domains inside the object having different refractive indexes. The phenomenon had been extensively used in the past for determining refractive coefficients and angles of total external reflection but not to investigate the internal structure of objects because of refraction (10^{-5} to 10^{-7}) is very difficult to examine. The possibility of inner structure investigations, using hard X-rays to reduce the related dose in the material and enhance the image quality due to the drop in the absorption at small wavelengths, leads to various attempts to obtain X-ray images using refraction phenomena. DEI will be applied to image the quality of the cork used for wine and other bottles. Various types of wood are used in preparing the cork for wine bottles. To manufacture good corks absolute quality rules must be applied for reliability. The present experimental work will explore

potential source of information based on visibility and provide sharp images with high contrast.

THEORY AND PRINCIPLES OF DEI

For hard X-rays (i.e., 20–70 keV) considerable transmission through thick body sections, the rocking curve width of a perfect silicon crystal is around 1 to 10 microradians, depending on the energy and the order of perfect crystal. The intensity of X-rays reaching the detector that have traversed a sample and have been diffracted by the analyzer can be expressed as

$$I = I_R R(\theta_0 + \theta_z), \tag{1}$$

where I_R is the intensity through the sample after attenuation is considered, R (θ) is the reflectivity of the crystal, θ_0 is the tuning angle of the analyzer, and $\Delta\theta_z$ is the refracting angle. The refracting angle, $\Delta\theta_z$, is defined as the angle in the plane of diffraction by which the X-rays deviate from the original direction while traversing the sample. Assuming there is no significant effect of small-angle scattering, $\Delta\theta_z$, can be derived by measuring the intensity of the X-rays transmitted through the sample and then diffracted by the analyzer, with the analyzer tuned to the shoulders of the rocking curve, once at the high-angle side, θ_H, and once at the low-angle side, θ_L, as shown in Fig. 1. It can be seen that the slope at the low-angle side or the high-angle side of the rocking curve is the steepest; the rocking curve can be approximated by

$$R(\theta_0 + \theta_z) = R(\theta_0) + (dR/d\theta)(\theta_0)\Delta\theta_z. \tag{2}$$

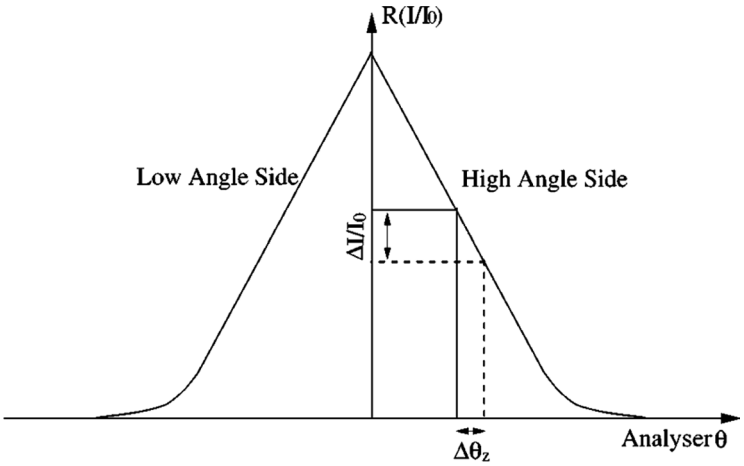

FIGURE 1. Physical principles of DEI. Variation of relative intensity with analyzer (θ) settings.

In DEI, two images are acquired, one from each side of the rocking curve because the absorption will be the same for each image, but the sensitivity to refraction will be of opposite signs due to the difference in the signs of the slopes on the two sides. Thus, the intensity of the images taken on the low-angle side (θ_L) and the high-angle side (θ_H) of the rocking curve are

$$I_L = I_R[R(\theta_L) + (dR/d\theta)(\theta_L)\Delta\theta_z] \tag{3}$$

$$I_H = I_R[R(\theta_H) + (dR/d\theta)(\theta_H)\Delta\theta_z]. \tag{4}$$

These two equations can be solved for the intensity affected by apparent absorption, I_R, and for the refraction angle image, $\Delta\theta_z$, the angle through which I_R is refracted in the z direction in traversing the object. The solutions are

$$I_R = I_L(dR/d\theta)(\theta_H) - I_H(dR/d\theta)(\theta_L)/R(\theta_L)(dR/d\theta)(\theta_H) - R(\theta_H)(dR/d\theta)(\theta_L) \tag{5}$$

$$\Delta\theta_z = I_H R(\theta_L) - I_L R(\theta_H)/I_L(dR/d\theta)(\theta_H) - I_H(dR/d\theta)(\theta_L). \tag{6}$$

In Eqs. (4) and (5), I_H and I_L are the intensities measured with the analyzer at θ_H and θ_L, respectively, R (θ) is the height of the rocking curve at the analyzer position θ, and ($dR/d\theta$) (θ_H) and ($dR/d\theta$) (θ_L) are the slopes of the rocking curves at (θ_H) and (θ_L), respectively. Equation (5) produces the apparent absorption image, because it contains both absorption and other extinction information about the sample and Eq. (6), when applied on a pixel-by-pixel basis to the DEI images, will produce a map of the refraction angle, refereed as the refraction image [25]. This analysis is applied to all the samples at different energies.

MATERIALS AND METHODS

The details of DEI technology and the associated instrumentation have been presented previously, and we will highlight the brief description. A schematic of the DEI system used for our experiments at the X15A beamline, NSLS, BNL, USA, is shown in Fig. 2.

The collimated fan beam of X-rays is prepared by the Silicon [3,3,3] monochromator consisting of two perfect silicon crystals. Once this beam passes through the subject, a third crystal (analyzer crystal) of the same reflection index diffracts the X-rays onto radiographic film (Kodak Professional Industrie 150, Industrex SR45) or an image plate detector (Fuji HRV image plate, read out by a Fuji BAS2500 image plate reader). The distance between the X-ray source and the specimen is approximately

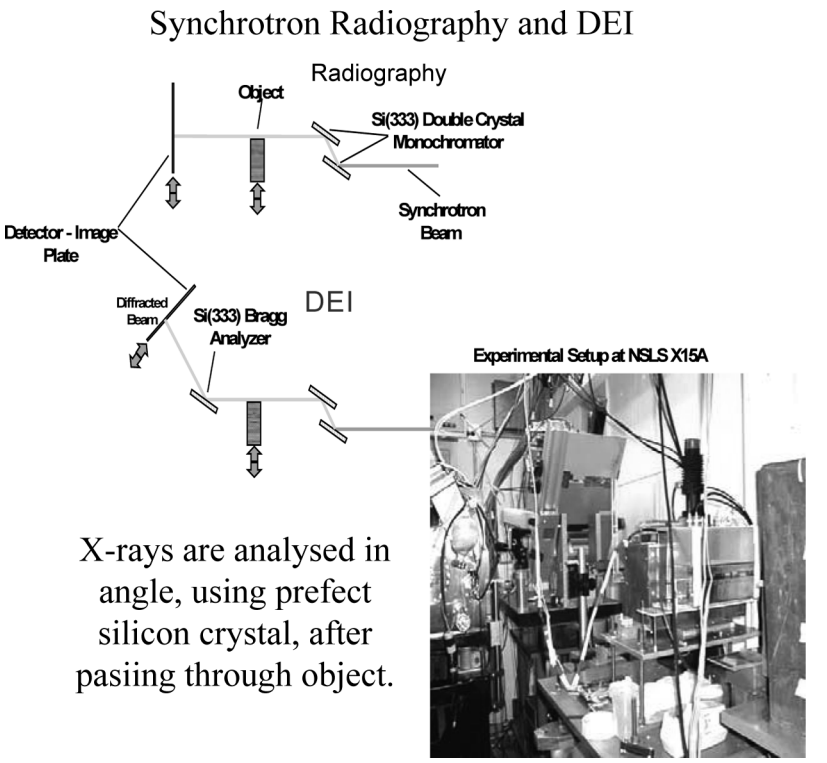

FIGURE 2. Experimental arrangement and the associated DEI/Conventional system.

20 m, while the distance between the specimens and the X-ray film or image plate detector is 1 m. The image of the subject is formed by scanning the subject and X-ray film at the same speed through the fan beam, in approximately opposite directions to take account of the Bragg reflection by the analyzer crystal. Because of the nondispersive nature of the crystals, the narrow Darwin-width of the diffraction used, and the small distance between the sample and the detector, the resolution of the image obtained is limited by the resolution of the X-ray film, which is approximately 50 μm, or the pixel size of the image plate detector, which is approximately 75 μm.

The Bragg condition for the analyzer crystal is met only when the incident beam makes the correct angle with the lattice planes in the crystal for a given X-ray energy. When this condition is met, the beam diffracts from the planes over a narrow range of incident angles. As the analyzer crystal is rotated about a horizontal plane, the crystal will go through a Bragg condition for diffraction and the diffracted intensity will trace out a profile or a rocking curve. The rocking curve of the analyzer in the protocol described here is roughly triangular and has peak intensity close to that of the beam

striking in it. The width of this profile is typically a few micro radians (the full width at half maximum is 1.5 micro radians at an X-ray energy of 40 keV and 3.6 micro radians at 18 keV, using the Si [3,3,3] reflection). This narrow angular width provides the tools necessary to prepare and analyze, on the micro radian scale, the angle of X-ray beams modified by the subject while traversing it. Since the range of the angles that can be accepted by the analyzer crystal is only a few micro radian, the analyzer crystal detects the subject's X-ray scattering (ultra-small-angle-scattering) and refraction of X-rays at the micro radian level, an angular sensitivity which is not possible in conventional radiography. The X-ray intensity in the subject is, therefore, modulated by the scattering and refraction properties of the subject. To extract refraction information, the analyzer is typically set to the half intensity points on the low and high angle sides of the rocking curve refereed to as -1 and $+1$, respectively, in the following discussion), or at the base of the rocking curve (refereed as -2 and $+2$, respectively, for the low and high angle sides), while the imaging takes place. For optimal extinction (scatter rejection) sensitivity, the analyzer is typically set to the peak of the rocking curve during imaging.

In addition, if two images are taken on the steepest slope of the reflectivity a so called absorption image and refraction image can be calculated. DEI relies on images recorded at well-known positions on the reflectivity curve of the analyzer crystal.

The reproducibility of the DEI images is maintained by monitoring the intensity of the diffracted X-rays by the analyzer just prior to imaging, to ensure that the analyzer is at the prescribed angular position. DEI system at 20, 30, and 40 keV with fixation of the sample is shown in Fig. 2. Diffraction enhanced techniques make use of the sample mounted on an x-y translation stage, so it can be a widely used method for materials testing.

All specimens were imaged in a medial to lateral direction at 20, 30, and 40 keV with DEI, and by conventional synchrotron X-ray radiography by removing the analyzer crystal and scanning the subject and detector through the monochromatic fan beam, at the same X-ray energy using the same X-ray dose as DEI. It should be noted that a conventional synchrotron X-ray image is of high quality in comparison to a non-synchrotron radiograph. Depending on the current of the electron storage ring, the dose delivered to the subject was measured with an ion chamber and maintained by adjusting the speed of each scan.

All scans are controlled by PC running a Windows-based C program. The program was specially written to control the DEI experiment. The program obtains from the user the type of scan, scan range, and analyzer positions, and performs the scan by controlling the image-plate motion (both horizontal and vertical), the sample's motion and the analyzer's position through the stepper motors. The program also monitors the ion-chamber response throughout the scan to obtain dose information and controls the shutter [26].

SPECIMENS

Natural cork provides unique physical properties that are perfectly suited for preservation and development of fine wine. Following the harvest, the bark is seasoned and sorted prior to processing. Seasoning allows the cork to stabilize and develop a uniform level of moisture. Cork's intricate cell structure creates a material that is compressible, resilient, and impervious. This type of cork withstands for environmental changes in heat, cold, and moisture. This benefits the wine by protecting against any leakage and early oxidation. They are then washed in a solution of hydrogen peroxide (H_2O_2) to bleach and sterilize the corks and eliminate microorganisms. After washing, the corks are dried in industrial ovens or with sterilized air to the correct moisture content. Finally, batches of corks are packed in polyethylene with sulfur dioxide (SO_2) gas, a widely-used preservative in the wine industry, and sealed in readiness for storage and shipping to cork distributors and wine producers around the world. A variety of chemicals are used to sanitize the corks against bacterial growth. Corks (dry) of above nature of various sizes are collected and stored and used for the acquisition of the images.

RESULTS AND DISCUSSION

Images of the cork obtained at 40 keV are shown in Figs. 3 to 6. Improved revealing features are observed in the images with high contrast. At optimum energy, it is possible to know the exact nature of the internal portion of the material. The difference of attenuation is more in weakly attenuating soft materials as distinguished from strongly attenuating materials. With optimum value of energy and improving the spatial resolution, the image contrast of the weakly attenuating materials such as cork can be improved considerably. The quality control of cork stoppers is mandatory in order to guarantee the

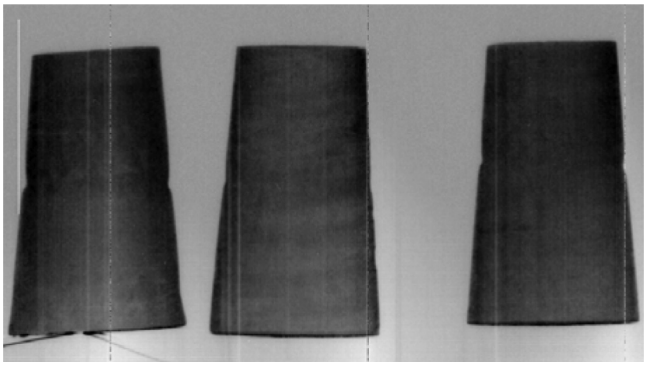

FIGURE 3. Images of the cork using 20 keV synchrotron X-rays.

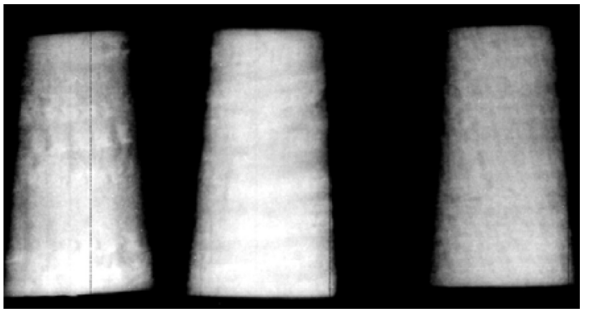

FIGURE 4. Images of the cork using 30 keV synchrotron X-rays.

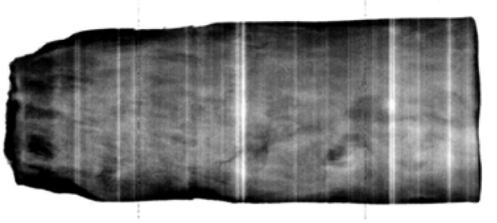

FIGURE 5. Image of the cork (smaller dimension) using 40 keV synchrotron X-rays.

perfect conservation of the wine. Several techniques have been developed, but until now the quality control was essentially related to the status of the external surface. Thus possible cracks, holes, and porosity inside the stopper will be hidden. The present technique put in evidence the presence of internal imperfections.

The images of the CT are shown in Figs. 7 to 8. In order to differentiate the soft material, we inserted the needle nearer to the center of the cork and simulated the image. The interior microstructure is clearly visible without

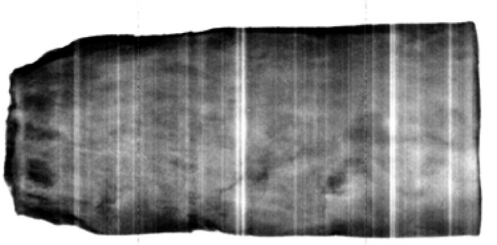

FIGURE 6. Image of the cork (larger dimension) using 40 keV synchrotron X-rays.

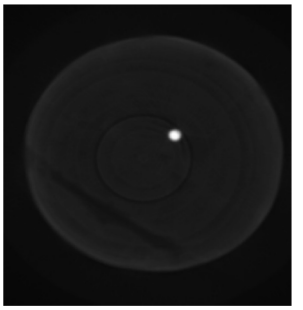

FIGURE 7. Image of the cork with insertion of the needle in CT mode. The tip of the needle and the crack have clear visibility compared to the conventional method.

any artifacts. Figure 8 shows the simulated image at 40 keV. In this way we differentiated the softly attenuating and weakly attenuation properties of the material with intense synchrotron X-rays and the later image is sharp with high contrast. Figures 9(a) to (c) show the refraction and absorption images at 18 and 36 keV, above and below K-absorption edge of iodine with the insertion of the needle for differentiating the attenuation of the hard material through soft-material. We examined and checked the DEI method for the present samples and studied the attenuation through a combination of weakly (cork) and strongly attenuating materials (by insertion of the needle nearer to the center of the cork).

The contrast in the refraction image (Fig. 9(a) to (b)) represents differences in intensity scattered through a particular angle. Thus attenuation differences are normally not apparent. Sources of contrast in the apparent absorption image (Fig. 9(c)) are absorption and extinction, scatter rejection. Extinction here means missing intensities of those X-rays that are scattered under angles substantially higher than the acceptance of the analyzer. X-ray photons deviate slightly, according to the variations of the real part of the refractive index, while traversing the sample. The minute refraction

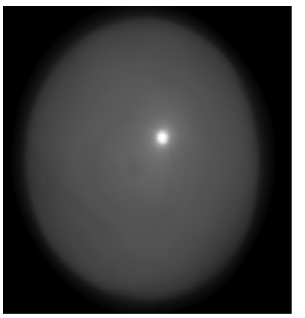

FIGURE 8. Simulated image of the cork at 40 keV with the tip of the needle.

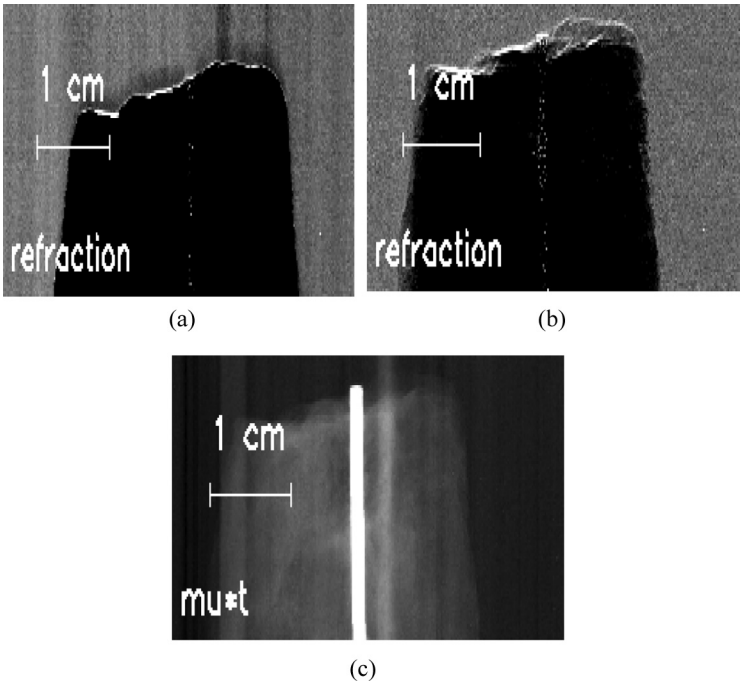

(a) (b)

(c)

FIGURE 9. (a)–(c) Refraction and absorption images at 18 and 36 keV with DEI.

angles for the biological material are in the order of micro-radians or tens of micro-radian. Figures 10 and 11 shows the corrected images at 18 keV and 36 keV. These images reflect the improvement of the contrast as distinguished from Fig. 9.

In DEI, the extinction contrast does not come from the X-rays being absorbed, but from the rejection of scattered X-rays. Since they are observed in the same way as the conventional radiography, the DEI image

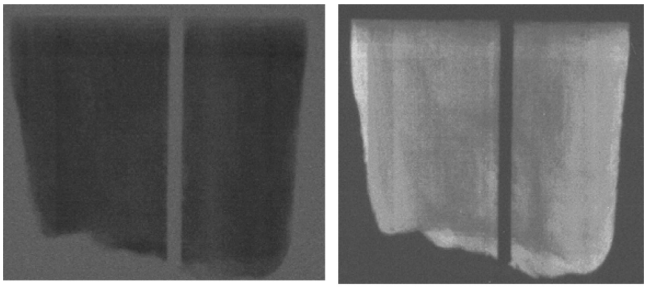

(a) (b)

FIGURE 10. (a) and (b) Corrected images at 18 keV with DEI.

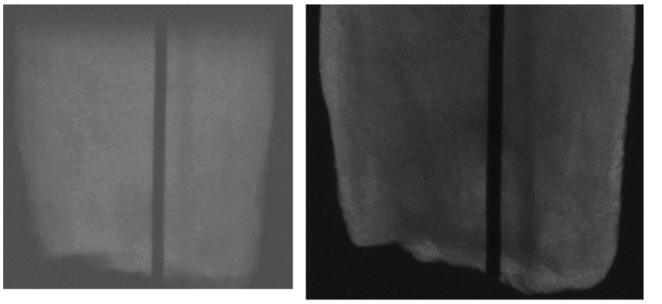

(a) (b)

FIGURE 11. (a) and (b) Corrected images at 36 keV with DEI.

dose is comparable to that in conventional radiography at the same X-ray energy. Thus the additional contrast comes without an additional dose to the subject.

For imaging the cork, in conventional radiography, absorption contrast is directly related to the dose received by the subject. More contrast means more absorbed X-rays which is proportional to the subject's dose. In DEI, the extinction contrast does not come from the X-rays being absorbed but from the rejection of scattered X-rays. Since they are observed in the same way as the conventional radiography, the DEI image dose is comparable to that in conventional radiography at the same X-ray energy. Thus the additional contrast comes without an additional dose to the subject. The sources of the contrast give a better understanding of the physics of DEI and opens up the possibility of improving the visualization and microstructure of a class of bio-materials invisible to radiography.

The present experimental study demonstrates the usage of the DEI to image the quality of the cork used for wine and other bottles. With DEI, good quality of images can be obtained in the field of material science. The goal of the present study was a preliminary exploration into the ability of the novel X-ray imaging technology, called DEI, to allow visualization of embedded cracks, holes, and porosity within the cork, with highly collimated synchrotron X-rays and exploring the application of DEI to image the soft-materials.

ACKNOWLEDGMENTS

One of the authors (DVR) analyzed the results by utilizing the facilities available at ICTP, Trieste, Italy, Istituto di Matematica e Fisica, Universita di Sassari, Sassari, Italy and the Department of Bio-Systems Engineering, Yamagata University, Japan. The travel support at the time of experiments was provided by DST, India, under the category of ''Utilization of Synchrotron Radiation and Neutron Scattering Facilities.''

REFERENCES

1. R. Fitzgerald. *Physics Today* **53**:23–26 (2000).
2. S. W. Wilkins, T. E. Gureyev, D. Gao, A. Pogany, and A. W. Stevenson. *Nature* **384**:335–338 (1996).
3. D. Chapman, W. Thomlinson, R. E. Johnston, D. Washburn, E. Pisano, N. Gmür, Z. Zhong, R. Menk, F. Arfelli, and D. Sayers. *Phys. Med. Biol.* **42**:2015–2025 (1997).
4. Z. Zhong, D. Chapman, R. Menk, J. Richardson, S. Theophanis, and W. Thomlinson. *Phys. Med. Biol.* **42**:1751–1762 (1997).
5. D. Chapman, E. Pisano, W. Thomlinson, Z. Zhong, R. E. Johnston, D. Washburn, and D. Sayers. *Breast Dis.* **10**:197–207 (1998).
6. C. Muehleman, D. L. Chapman, K. E. Kuettner, J. Rieff, J. A. Mollenhauer, K. Massuda, and Z. Zhong. *The Anatomical Record Part. A* **272**:392–397 (2003).
7. O. Oltulu, Z. Zhong, M. Hasnah, M. N. Wernick, and D. Chapman. *J. Phys. D: Appl. Phys.* **36**:2152–2156 (2003).
8. J. Li, Z. Zhong, R. Lidtke, K. E. Kuettner, C. Peterfy, E. Aliyeva, and C. Muehleman. *J. Ant.* **202**:463–470 (2003).
9. R. A. Lewis, C. J. Hall, A. P. Hufton, S. Evans, R. H. Menk, F. Arfelli, L. Rigon, G. Tromba, D. R. Dance, I. O. Ellis, A. Evans, E. Jacobs, S. E. Pinder, and K. D. Rogers. *The Bri. Jour. Radio* **76**:301–308 (2003).
10. M. Z. Kiss, D. E. Sayers, Z. Zhong, C. Parham, and E. Pisani. *Phys. Med. Biol.* **49**:3427–3439 (2004).
11. D. V. Rao, T. Yuasa, T. Akatsuka, Z. Zhong, G. Tromba, and T. Takeda. Proceedings of the 8th International Conference on X-ray Microscopy, 26–30th July, Egret, Himaji, Japan, 235–236 (2005).
12. M. Kelly, R. Beavis, D. Fourney, E. Schultke, C. Parham, B. Juurlink, Z. Zhong, and D. L. Chapman. *Can. Assoc. Radiol. J.* **57**:204–210 (2006).
13. C. Kim, M. Bourham, and J. A. Doster. *Nucl. Instrum. Meth. A* **566**:713–721 (2006).
14. C. Muehleman, J. Li, and Z. Zhong. *Osteoarthr. Cartilage* **14**:882–888 (2006).
15. A. Antunes, A. Safatle, P. Barros, and S. Morelhao. *Med. Phys.* **33**:2338–2343 (2006).
16. D. Connor, D. Sayers, D. Sumner, and Z. Zhong. *Phys. Med. Biol.* **51**:3283–3300 (2006).
17. M. Wernick, Y. Yang, I. Mondal, D. Chapman, M. Hasnah, C. Parham, E. Pisano, and Z. Zhong. *Phys. Med. Biol.* **51**:1769–1778 (2006).
18. G. Khelashvili, J. Brankov, D. Chapman, M. Anastasio, Y. Yang, Z. Zhong, and M. Wernick. *Phys. Med. Bio.* **51**:221–236 (2006).
19. J. Brankov, M. Wernick, Y. Yang, J. Li, C. Muehleman, Z. Zhong, and M. Anastasio. *Med. Phys.* **33**:278–289 (2006).
20. C. Muehleman, J. Li, Z. Zhong, J. Brankov, and M. Wernick. *J. Anatomy* **208**:115–124 (2006).
21. C. Chou, M. Anastasio, J. Brankov, M. Wernick, E. Brey, D. Connor Jr., and Z. Zhong. *Phys. Med. Biol.* **52**:1923–1945 (2007).
22. M. Hasnah, Z. Zhong, C. Parham, H. Zhang, and D. Chapman. *Nucl. Instrum. Meth. A* **572**:953–957 (2007).
23. L. W. Young, C. Parham, Z. Zhong, D. Chapman, D. Reaney, and J. T. Martin. *J. Exp. Bot.* **58**:2513–2523 (2007).
24. D. V. Rao, Z. Zhong, and G. Tromba. Proceedings of the 15th International Conference on Vacuum Ultraviolet Radiation Physics, July 29th–August 3rd, 2007. Berlin, Germany. Book of proceedings of Abstracts: Imaging and Microscopy, p. 65.
25. M. Z. Kiss, D. E. Sayers, and Z. Zhong. *Phys. Med. Bio.* **48**:325 (2003).
26. Z. Zhong, W. Thomlinson, D. Chapman, and D. Sayers. *NIM A* **450**:556 (2000).